Journal of Thermal Analysis and Calorimetry
https://doi.org/10.1007/s10973-024-13180-x

Numerical study of the effect of aspect ratio on the entropy generation due to Rayleigh–Benard convection in 2D trapezoidal cavity

Sardar Bilal[1] · Noor Zeb Khan[2] · Ali Akgül[3,4]

Received: 12 August 2023 / Accepted: 4 April 2024

Abstract
The investigation of entropic variations in the thermal transport mechanism produced by buoyantly driven temperature gradients has attracted significant attention because of excellent physical significance. Therefore, the prime consent to manipulate the current investigation is to explore the impact of change in the aspect ratio of the trapezoidal cavity in the optimization of the entropy phenomenon. After attaining motivation from its practical essence different entropies including thermal, viscous, and local are estimated. Additionally, global quantities such as average Bejan and Nusselt numbers calculated along with total entropy are measured against flow concerning parameters (aspect ratio (AR), Rayleigh number (Ra) and irreversibility ratio (ϕ)). Numerical experiments are performed by implementing a finite element approach using open-source software renowned as COMSOL Multiphysics. Before the accomplishment of the outcomes, confirmation of the numerical technique is assured by establishing grid sensitivity testing. Comparison of results between present and previous studies is also demonstrated. A wide range of involved sundry parameters varying from $10^{-4} \leq \phi \leq 10^{-2}$, $10^2 \leq \mathrm{Ra} \leq 10^5$ and $0.25 \leq \mathrm{AR} \leq 0.75$ are accounted. It is concluded that by escalating the aspect ratio from 0.50 to 0.75, the magnitude of the local entropy enhances from 3370 to 3424. It is revealed that the highest value of viscous entropy that is, 45, is achieved at $\mathrm{Ra} = 10^5$ and by keeping the aspect ratio of enclosure equal to 0.75, whereas, the thermal entropy approaches 2 for the same situation of parameters. The magnitude of the average Bejan number reaches unity at $\mathrm{AR} = 0.5$ and $\mathrm{Ra} = 10^5$, whereas for low and high aspect ratios it depicts a magnitude less than 1 for the same Rayleigh number.

Keywords Entropy generation (EG) · Trapezoidal enclosure · Aspect ratio · Natural convection · Newtonian fluid · FEM

List of symbols

(x, y)	Dimensional horizontal and vertical coordinates (m)
(ξ, ς)	Dimensionless horizontal and vertical coordinates
(u, v)	Dimensional horizontal and vertical velocity components (ms^{-1})
(β, γ)	Dimensionless horizontal and vertical velocity components
p	Dimensional pressure (Pa)
P	Dimensionless pressure
H	Height of the cavity (m)
W	Length of the cavity (m)
T_c	Temperature at cold wall (K)
T_h	Temperature at hot wall (K)
$\Im$	Dimensionless temperature
G	Gravitational force (ms^{-2})
β^*	Thermal expansion (K^{-1})
α	Thermal diffusivity $(\mathrm{m}^2\mathrm{s}^{-1})$

✉ Ali Akgül
aliakgul00727@gmail.com

Sardar Bilal
sardarbilal111@yahoo.com

Noor Zeb Khan
noor.zeb722@gmail.com

[1] Department of Mechanical Engineering, College of Engineering, Prince Mohammad Bin Fahd University, Al Khobar, Saudi Arabia

[2] Department of Mathematics, Air University, Sector E-9, Islamabad, Pakistan

[3] Department of Computer Science and Mathematics, Lebanese American University, Beirut, Lebanon

[4] Department of Mathematics, Art and Science Faculty, Siirt University, 56100 Siirt, Turkey

Published online: 29 April 2024

ν	Kinematic viscosity (m^2s^{-1})
ϕ	Irreversibility distribution ratio
C_p	Specific heat capacity ($Jkg^{-1}K^{-1}$)
K	Thermal conductivity ($Wm^{-1}K^{-1}$)
μ	Dynamic viscosity ($kgm^{-1}s^{-1}$)
ρ	Density (kgm^{-3})
AR	Aspect ratio (H/L)
Si	Local entropy (JK^{-1})
$Si_{thermal}$	Thermal entropy (JK^{-1})
$Si_{viscous}$	Viscous entropy (JK^{-1})
Si_{Total}	Total entropy (JK^{-1})
Nu	Local Nusselt number along surface of heated walls
Nu_{Avg}	Average Nusselt number
Ra	Rayleigh number
Pr	Prandtl number
Be	Bejan number
Be_{Avg}	Average Bejan number

Introduction

Energy transmission in closed configurations occurs due to thermodynamic changes imparted by convective transport. The optimization of heat transfer management in confined geometries to attain efficient energy systems is a requirement of the ongoing technological era. Additionally, the reduction and control of energy losses in such systems are strategized by measuring entropic variations. The entropy in any thermalized system is subjected to heat and mass variations, frictional forces, and buoyancy aspects. The assessment of any engineering framework is scrutinized by formulating entropy aspects. Owing to the aforementioned physical significance, much attention has been paid in recent years to the fields of turbomachinery, electronic cooling, heat exchangers, combustion processes, heat engines and pumps, refrigerators, cooling systems, power plants, etc. Some recent developments in the investigation of entropy measurements in the hydrothermal flow of fluids are described here. Like, Dagtekin et al. [1] delineated that at a low thermal Rayleigh number magnitude, the conduction regime plays a crucial role in the generation of entropy, while at high values of (Ra), convection serves as the primary source in entropy generation. Numerical experiments to examine the entropy state in transiently formulated laminar flow of fluid saturated in the enclosure along with the provision of differentially heated boundaries were executed by Magherbi et al. [2]. Measurement of different types of entropy along with a global quantity named total entropy in free convective transport by implementing the finite element procedure was manifested by Yilbas et al. [3]. Erbay et al. [4, 5] determined the role of partially distributed activated thermalized vertically lateral walls in producing irreversibility in buoyantly driven transport in a square enclosure to measure energy losses. Strategies to minimize entropy production via inclination effects of enclosure and control it through the reduction of frictional and buoyancy forces were enclosed by Baytas [6]. Andreozzi et al. [7] estimated about productivity rate of local and global entropy for convective transport in a heated channel saturated with air by prescribing uniform heat flux. Mahmud and Islam [8] delineated the role of corrugated boundaries in managing entropy distribution in laminar free convective flow in a cavity by performing a computational scheme. Deviation in field variables such as velocity and temperature in the flow of viscous liquid in a square enclosure containing solid objects inside with entropy phenomenon was explicated by Shuja et al. [9]. Generation of entropy measurement during assembly of gold and silver via short pulse laser heating was experimentally calculated by Yilbas [10]. Hijleh et al. [11, 12] investigated the irreversibility process in viscous fluid flow in a helical coil by providing uniform heat flux along with the insertion of highly thermally conductive fins. Mathematical formulation to envision new factors affecting the entropy phenomenon by employing irreversibility law was presented by Naterer et al. [13].

Optimization in the performance of fluid-based systems can be achieved by altering the aspect of enclosures. The adjustment of thermal gradients and flow patterns to maximize the heat transfer existing between boundaries and fluid is also handled by aspect ratio variations of confined domains. Changing the aspect ratio of enclosures can have various applications in different fields. Mixing efficiency of fluids, which yields the quality of bio products in chemical processes and bioreactors is also managed by aspect ratio deviation of cavities. Some more real-life utilization of geometries with shape change aspects are involved in, electronic cooling, heat exchangers, aircraft designing, and many more. Hydrothermal attributes of natural convective flow by making changes in the aspect ratio of an inclined enclosure filled with viscous fluid by employing finite difference simulations were executed by Cheong et al. [14]. Change in aspect ratio via the varying length of the base and adjacent walls of the permeable square cavity and by altering thermal boundary constraints was investigated by Ramakrishna et al. [15]. Sheikholeslami et al. [16] delineated flow and thermal behavior of water-based nanoliquid with magnetic field implementation and by making variation in the aspect ratio of the enclosure. Mejri et al. [17] analyzed the magnetized free convective flow of a nanoliquid with entropy production in a cavity whose aspect ratio and strength of the magnetic source were varied.

Distribution of energy in confined domains due to the existence of temperature gradient causes natural convection. Consequence, volumetric changes are produced. A wide range

of applications concerning naturally convective flow has been witnessed in different engineering processes such as cooling of electronic gadgets, insulating double glazed windows, solar panels, etc. Several interesting studies on free convection with multiple physical influences have been conducted. For the sake of brevity, a few of them are described here, for example, natural convection in a rectangular cavity with the effectiveness of heater placement at vertical boundaries of a square chamber was examined by Catton [18]. Davis [19] developed mathematical framework to discuss the factors controlling free convection, along with the inclusion of body forces. Ostarch [20] carried out a computational analysis of buoyantly driven viscous liquid flow saturated in an enclosure using concept of heat lines. Free convection in a non-Newtonian fluid incorporating the aspect of low thermal Rayleigh number explaining variable thermal conductivity features in the square cavity was adumbrated by Emery and Lee [21]. Representation of flow structures development through stream and heat lines for convective flow in the isothermal cavity was visualized by Aydin et al. [22]. Turan et al. [23] explored the influence of uniform and non-uniform heating on steady and laminar convective flow in rectangular enclosures using a computational scheme. Deviation in heat flux related to the fluid motion and heat transfer in cylindrical chamber, was explored by Ganguli et al. [24]. The latest developments in hydrothermal characteristics imparted by convective transport are encapsulated in refs. [25–29].

The formation of vortices and isothermal fields against variations in the aspect ratio of the enclosure has received tremendous attention from researchers due to overwhelming utilization. Additionally, entropy generation is also managed by such changes which contain potential significance. From the aforementioned cited works, it is concluded that no joint studies have been conducted so far which involve the change of aspect ratio and entropy phenomenon together. To fill this gap, a novel effort has been performed in the present study, which includes the measurement of the entropy process via signifying aspects of local, thermal, and viscous entropies. A wide range of involved parameters is utilized to provide a comprehensive study that assists others in conducting research in this direction. Graphical representations are used to examine total entropy production against aspect ratio. Bejan number showing the ratio of thermal to flow friction entropies is also calculated.

Mathematical formulation

Definition of the problem

Let us assume 2D, incompressible (ρ = constant), steady ($t = 0$) and laminar flow of Newtonian fluid in trapezoidal enclosure with two vertically non-parallel adiabatic walls and uniformly heated base and top boundaries. The top wall is provided with cooled temperature (T_c), and uniform temperature (T_h) is prescribed at bottom wall, while inclined walls are kept insulated ($\frac{\partial T}{\partial n} = 0$). The Boussinesq approximation is used to formulate persistent fluid density. Aspect ratio (AR) is defined by the fraction of height (H) of the vertical wall to the length (L) of the horizontally wall. The graphical visualization of domain is depicted in Fig. 1.

Constitutive equations

The governing equations for mass, momentum, and energy under considered physical assumptions indicated above are described as under [2].

$$u_x + v_y = 0 \tag{1}$$

$$uu_x + vu_y + \frac{1}{\rho}p_x = \upsilon\left(u_{xx} + u_{yy}\right) \tag{2}$$

$$uv_x + vv_y + \frac{1}{\rho}p_y = \upsilon\left(v_{xx} + v_{yy}\right) + g\beta^*\left(T - T_c\right) \tag{3}$$

$$uT_x + vT_y = \alpha\left(T_{xx} + T_{yy}\right) \tag{4}$$

Following parameters are capitalized to change above dimensional governing system in to dimensionless form

$$x = \frac{\xi}{L},\ y = \frac{\varsigma}{L},\ u = \frac{\beta}{\alpha L},\ v = \frac{\gamma}{\alpha L},$$
$$\mathfrak{F} = \frac{\left(-T_c + T\right)}{\left(-T_c + T_h\right)},\ P = \frac{pL^2}{\rho\alpha^2},\ \Delta T = -T_c + T_h \tag{5}$$

Non-dimensionalized version of constitutive expressions are described as below [2]

$$\beta_\xi + \gamma_\varsigma = 0 \tag{6}$$

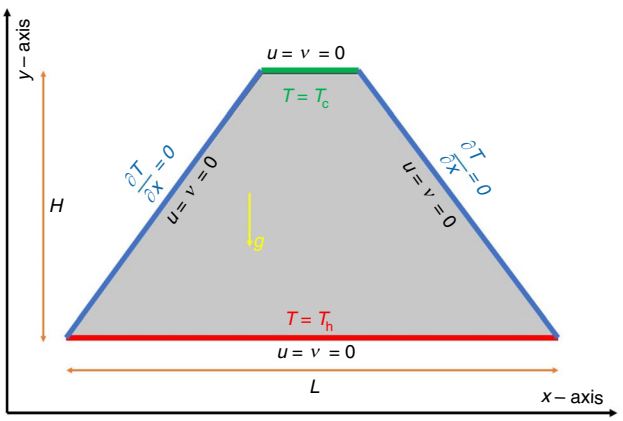

Fig. 1 Geometric physical model and 2-D cartesian coordinates

$$\beta\beta_{\xi} + \gamma\beta_{\varsigma} + P_{\xi} = \Pr\left(\beta_{\xi\xi} + \beta_{\varsigma\varsigma}\right) \tag{7}$$

$$\beta\gamma_{\xi} + \gamma\gamma_{\varsigma} + P_{\varsigma} = \Pr\left(\gamma_{\xi\xi} + \gamma_{\varsigma\varsigma}\right) + \Pr \mathrm{Ra}\mathfrak{T} \tag{8}$$

$$\beta\mathfrak{T}_{\xi} + \gamma\mathfrak{T}_{\varsigma} = \mathfrak{T}_{\xi\xi} + \mathfrak{T}_{\varsigma\varsigma} \tag{9}$$

Involved physical parameters are mentioned as below.
$\Pr = \frac{\upsilon}{\alpha}$, $\mathrm{Ra} = \frac{g\beta^{*}\Delta TL^{3}}{\upsilon\alpha}$.
Associated boundary constrains are presented as under.
At the heated bottom wall: $\mathfrak{T} = 0.5$, $\beta = \gamma = 0$,
At the insulated side walls:

$$\frac{\partial\mathfrak{T}}{\partial n} = 0,\ \beta = \gamma = 0 \tag{10}$$

At the cold top wall: $\mathfrak{T} = -0.5$, $\beta = \gamma = 0$.

Entropy generation

Mathematical expressions related to local entropy based on equilibrium state between thermal and fluid frictional forces are shown as under

$$\mathrm{Si}_{\mathrm{Thermal}} = \left[\left(\mathfrak{T}_{\xi}\right)^{2} + \left(\mathfrak{T}_{\varsigma}\right)^{2}\right] \tag{11}$$

$$\mathrm{Si}_{\mathrm{Viscous}} = \phi\left[2\left(\beta_{\xi}\right)^{2} + 2\left(\gamma_{\varsigma}\right)^{2}\right] + \left[\left(\beta_{\varsigma} + \gamma_{\xi}\right)^{2}\right] \tag{12}$$

Local entropy formulation number also known as the entropy formulation number is produced by adding $\mathrm{Si}_{\mathrm{Thermal}}$ and $\mathrm{Si}_{\mathrm{Viscous}}$:

$$\begin{aligned}\mathrm{Si} = \mathrm{Si}_{\mathrm{Thermal}} + \mathrm{Si}_{\mathrm{Viscous}} = \mathrm{Si} = &\left[\left(\mathfrak{T}_{\xi}\right)^{2} + \left(\mathfrak{T}_{\varsigma}\right)^{2}\right] \\ &+ \phi\left[2\left(\beta_{\xi}\right)^{2} + 2\left(\gamma_{\varsigma}\right)^{2}\right] + \left[\left(\beta_{\varsigma} + \gamma_{\xi}\right)^{2}\right]\end{aligned} \tag{13}$$

where, ϕ is the ratio of the irreversibility distribution:

$$\phi = \frac{\mathrm{Si}_{\mathrm{Viscous}}}{\mathrm{Si}_{\mathrm{Thermal}}} = \frac{\mu T_{o}}{k}\left(\frac{\alpha}{L\Delta T}\right)^{2} \tag{14}$$

Formulation of global quantity (total entropy) is expressed as under.

$$\begin{aligned}\mathrm{Si}_{\mathrm{Total\ \ Thermal}} &= \iint_{V} \mathrm{Si}_{\mathrm{Thermal}}\mathrm{d}V \\ \mathrm{Si}_{\mathrm{Total\ \ Viscous}} &= \iint_{V} \mathrm{Si}_{\mathrm{Viscous}}\mathrm{d}V \\ \mathrm{Si}_{\mathrm{Total}} &= \mathrm{Si}_{\mathrm{Total\ \ Thermal}} + \mathrm{Si}_{\mathrm{Total\ \ Viscous}}\end{aligned} \tag{15}$$

Quantities of interest

Bejan number (Be)

The strength of the $\mathrm{Si}_{\mathrm{Thermal}}$ reversibility is indicated by the Bejan number (*Be*) as referred in [2]

$$\mathrm{Be} = \frac{\mathrm{Si}_{\mathrm{Thermal}}}{\mathrm{Si}} \tag{16}$$

If $\mathrm{Be} > 1/2$ heat transport irreversibility is dominant, whereas if $\mathrm{Be} < 1/2$, friction of fluid irreversibility is dominant. Heat transport and viscous irreversibilities are identical for $\mathrm{Be} = 1/2$. The importance of thermal transport due to entropy is highlighted by measuring average Bejan number $\left(\mathrm{Be}_{\mathrm{Avg}}\right)$ which is expressed mathematically as under

$$\mathrm{Be}_{\mathrm{Avg}} = \iint_{V} \mathrm{Si}_{\mathrm{Total\ \ thermal}}/\mathrm{Si}_{\mathrm{Total}}\mathrm{d}V \tag{17}$$

Nusselt number (Nu)

The thermal transport characteristics are assessed through the Nusselt number calculated at the nanofluid interface as follows:
$\mathrm{Nu}_{\mathrm{Local}} = \frac{\partial\mathfrak{T}}{\partial y}$,
By integrating the heated surface, the $\mathrm{Nu}_{\mathrm{Avg}}$ is evaluated and is expressed as:

$$\mathrm{Nu}_{\mathrm{Avg}} = \int_{S} \mathrm{Nu}_{\mathrm{Local}}\mathrm{d}S \tag{18}$$

Here, the heated surface is represented by *S*.

Ecological coefficient of performance (ECOP)

It is defined as an evaluation criterion for estimating thermal performance of cavity. ECOP is recognized as the ratio of the average Nusselt number to total entropy generation and is based on second thermodynamics law. It is an essential physical quantity and increase in ECOP is desirable for efficient thermal systems. ECOP is defined as follow.

$$\mathrm{ECOP} = \frac{\mathrm{Nu}_{\mathrm{Avg}}}{\mathrm{Si}_{\mathrm{Total}}} \tag{19}$$

Kinetic energy (K.E.)

The computation to assess the total kinetic energy (K.E.) is determined by using the following equation:

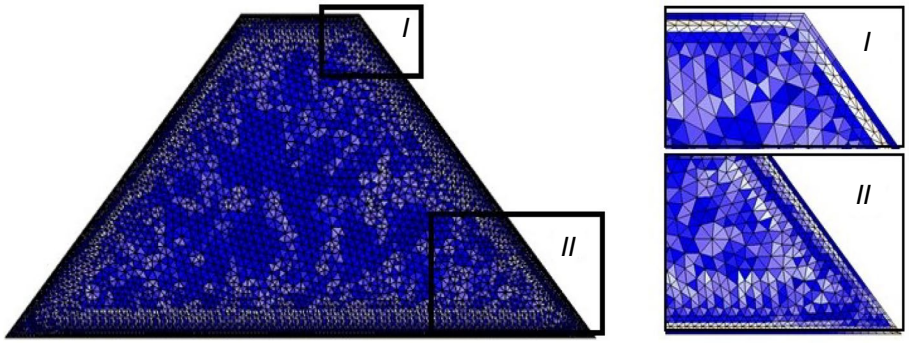

Fig. 2 Grid formation of domain at extra fine level

$$\text{K.E.} = \frac{1}{2}\int_{\Omega} \mathbb{Q}^2 d\Omega \tag{20}$$

Here, the velocity vector is represented as $\mathbb{Q} = (\beta, \gamma)$.

Solution methodology

Mesh generation

In computational procedure, it is essential to describe the considered physical configuration and the subdivision of present domain into sub-portion (element) is known as meshing. In finite element approach, 2D structures are divided into triangular and rectangular elements which is another advantage over finite difference and volume techniques. Furthermore, these elements are connected with characteristics points recognized as nodes. At each node the number of field variables are called as degree of freedom. The displacement of node in each element is dependent on selection of refinement method which is hybrid meshing in present study and known as hp refinement. It involves a combination of h-refinement (splitting elements into smaller sub-elements) and p-refinement (increasing the degree of the polynomials used to approximate the solution within each element). This approach allows for a more adaptive and efficient way to refine the mesh, as it can target areas where the solution is changing rapidly or where the error is large. The hp-refinement process can be guided by error indicators, which help determine the optimal combination of h- and p-refinement for each element. This approach can lead to faster convergence and provide more accurate results in comparison to traditional h, p, and r-refinements**.** Figure 2 delineates the meshing of current design (trapezoidal enclosure) at extra fine level.

Grid sensitivity test

In order to attain solution independent of mesh variations it is compulsory to perform grid independent test which will provide the assurance of simulated experiments as well as show the credibility of capitalized procedure (F.E.M). For this purpose, Table 1 is presented which expresses the variation in kinetic energy (K.E.) and average Bejan number (Be_{Avg}) at different mesh levels by restricting $\text{Pr} = 0.71$, $\text{AR} = 0.50$, $\phi = 10^{-2}$ and $\text{Ra} = 10^5$. From the statistics of attained results, it is seen that values of both physical quantities match at R.L-8 and R.L-9. These outcomes adhere that all the simulations are accounted at R.L-8 to reduce computational and time expenditures.

Table 1 Meshing at different refinement levels

R. levels	No. of elements	DOF	K.E./J	Be_{Avg}
R.L-1	239	760	559.37	0.00093142
R.L-2	414	1243	626.00	0.0022469
R.L-3	640	1807	733.35	0.0021212
R.L-4	1196	3185	843.45	0.0020831
R.L-5	1835	4680	966.22	0.0020718
R.L-6	3017	7296	1033.0	0.0022829
R.L-7	8149	18,988	1048.9	0.0025850
R.L-8	20,887	46,970	1048.9	0.0025850
R.L-9	31,949	69,094	1048.9	0.0025850

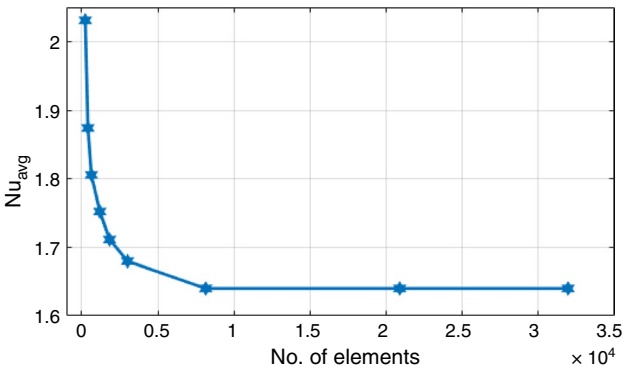

Fig. 3 Grid convergence test for Nu_{Avg}

In addition, to ensure the effectiveness of grid formation at different refinement levels, Nusselt number (Nu_{Avg}) is also sketched against change in number of elements (see Fig. 3). From the display portray, it is found that with rise in number of elements, the average Nusselt number coincides. During the accomplishment of (Nu_{Avg}), other involved parameters are constrained at Pr = 0.71, $\phi = 10^{-2}$ and Ra = 10^5.

Validation of results

Verification about findings of present investigation is ensured by matching comparison for outcome of average Nusselt number with results published by Saeid and Pop [30] and Poulikakos [31] against change in Rayleigh number (Ra). Here, (Ra) is varied from 100 to 1000 and Prandtl number (Pr) is fixed by 0.7. from the attained outcomes and percentage deviation presented in Table 2, an excellent agreement between existing and current work is developed.

Results and interpretation

This segment is presented to explore and interpret the impact of variation in aspect ratio of computational domain along with involved physical parameters on hydrothermal properties and entropy generated by convective transport mechanism in trapezoidal enclosure. For this purpose, finite element simulations are performed to attain outcomes of present study. To examine entropic variations in exclusive manner two types of entropies (viscous and thermal) are accounted. In addition, global (total entropy) and local (local entropy and Nusselt number) quantities are also analyzed. Subsequently, ECOP determining the performance of considered physical domain and Bejan number signifying the ratio between thermal and local entropies is also evaluated against involved parameters. Figure 4a–f interprets the behavior of velocity and temperature fields along with measurement of viscous, thermal and local entropies and Bejan number at AR = 0.50, Ra = 10^3, and $\phi = 10^{-4}$ is presented. Figure 4a exhibits vortex formation in domain via stream lines representation. Cells of two equivalent size and symmetrical in shape but in opposite orientation are formed and covers complete space of the domain. Flow circulations in left cell is in clockwise direction, whereas in right, one fluid rotates in anticlockwise orientation. Maximum magnitude of stream function $\psi_{max} = 0.07$ is attained near the center of cavity. In Fig. 4b, it is noticed that isothermal contours are almost parallel to horizontal bottom wall which is uniformly heated and shows the dominance of heat transport through conduction instead of convection due to the less production of buoyancy forces. Entropy generated due to the transmission of heat and friction developed by flow of fluid are sketched and displayed in Fig. 4c, d. Maximum magnitude of thermal entropy revealed is 74.7, while value of local viscous entropy reduces to 0.06369. The reason behind such maximum and minimum scale of both entropies is because of the fact that (Ra) induces convective potential between heated and colder zones of domain due to which thermal gradients dominate over momentum diffusions. Figure 4e explains the response of local entropy against thermal Rayleigh number (Ra) and by fixing other parameters. Since, local entropy signifies the sum of thermal and viscous entropies due to which it is high and intense near the cold boundary of enclosure. Deviation in Bejan number (Be) at low magnitude of Rayleigh number (Ra = 10^3), AR = 0.50 and $\phi = 10^{-4}$ is seen in Fig. 4f. It is manifested that near the heated boundaries it reaches to unity because here thermal conduction dominates over viscous diffusion.

In Fig. 5, streamlines, isotherms, $Si_{Thermal}$, $Si_{Viscous}$, Si, and Be are analyzed for $\phi = 10^{-4}$ AR = 0.5 and Ra = 10^5. Two symmetrical cells near top wall are produced covering region between bottom wall and middle of cavity, as shown by the streamlines are plotted in Fig. 5a. Magnitude of stream function rises up to $\psi_{max} = 0.08$ due to intensification in the strength of buoyancy forces produced because of thermal convective potential. From the comparison of isotherms formed in Fig. 4b and 5b, it is observed that convective heat transport is enhanced in the cavity as Rayleigh number (Ra) is increased. Furthermore, it is obtained that isothermal contours become distorted and non-parallel to horizontal bottom wall which predict the dominance of convective potential. Figure 5c, d shows comparison of thermal and viscous entropies and found that friction of fluid is significantly higher than the local entropy formulation due to heat transport. Entropy generation caused by heat transport can reach a maximum value of $\left(Si_{Thermal}\right)_{Max} = 365$, whereas fluid friction can reach $\left(Si_{Viscous}\right)_{Max} = 3360$. Figure 5e expresses the impact of high thermal Rayleigh number (Ra = 10^5) on local

Table 2 Comparison of average Nusselt number against Rayleigh number for both the current and previous studies

Ra	Nu_{Avg}		
	Saeid and Pop [30]	Poulikakos [31]	Present work
100	1.162 (0.086%)	1.160 (0.086%)	1.161
200	1.486 (0.067%)	1.484 (0.067%)	1.485
300	1.830 (0.054%)	1.828 (0.054%)	1.829
400	2.308 (0.043%)	2.306 (0.043%)	2.307
500	2.455 (0.040%)	2.453 (0.040%)	2.454
600	3.174 (0.063%)	3.170 (0.063%)	3.172
700	3.515 (0.056%)	3.512 (0.028%)	3.513
800	3.725 (0.053%)	3.720 (0.080%)	3.723
900	3.986 (0.025%)	3.982 (0.075%)	3.985
1000	4.156 (0.048%)	4.151 (0.072%)	4.154

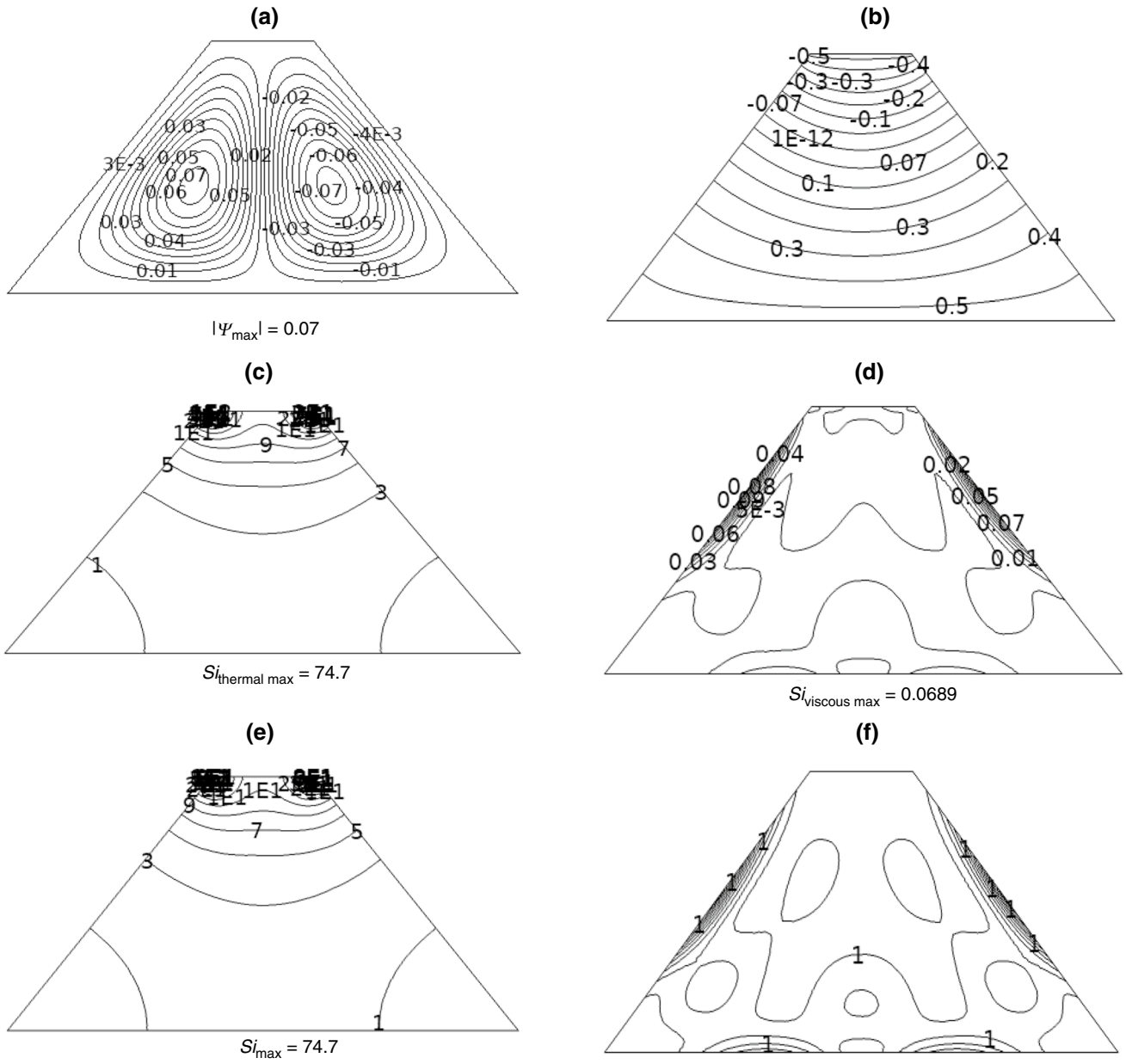

Fig. 4 Variations in **a** streamlines, **b** isotherms, c $Si_{Thermal}$, **d** $Si_{Viscous}$, **e** Si and **f** Be contours at AR = 0.50, Ra = 10^3, and $\phi = 10^{-4}$

entropy. From the sketch of local entropy generation contours similarity with fluid friction entropy maps ($Si_{Viscous}$) is depicted. This consequence, provide evidence about dominating role of friction forces in generating irreversibility. Figure 5f, demonstrates the distribution of local Bejan number (Be) in the enclosure which illustrates the dominance of irreversibility due to fluid friction. The outcomes revealed that the local Bejan number (Be) ranges from 0 to 1.

Figure 6 illustrates behavior of streamlines, isotherm contours, thermal entropy, viscous entropy and local Bejan number at AR = 0.75, $\phi = 10^{-4}$, and Ra = 10^5. Figure 6a envision streamlines and observes two symmetrical cells at top and at the middle of bottom wall. It is revealed that by incrementing aspect ratio of enclosure magnitude of stream function rises up to ψ_{max}= 8 which justifies that increase in aspect ratio causes up left in the strength of velocity field rises. It is because of the argument that by increasing aspect ratio of enclosure up to 0.75 provides space to the fluid for motion and as an outcome the factor of shear stress also enriches. Figure 6b represents variation in isothermal contours at AR = 0.75,$\phi = 10^{-4}$, and Ra = 10^5. From the isothermal contours' formation, it is noticed that, increase in aspect ratio produces diffusion of heat from heated to colder regions. Here, it is worthwhile to mention that by elevating

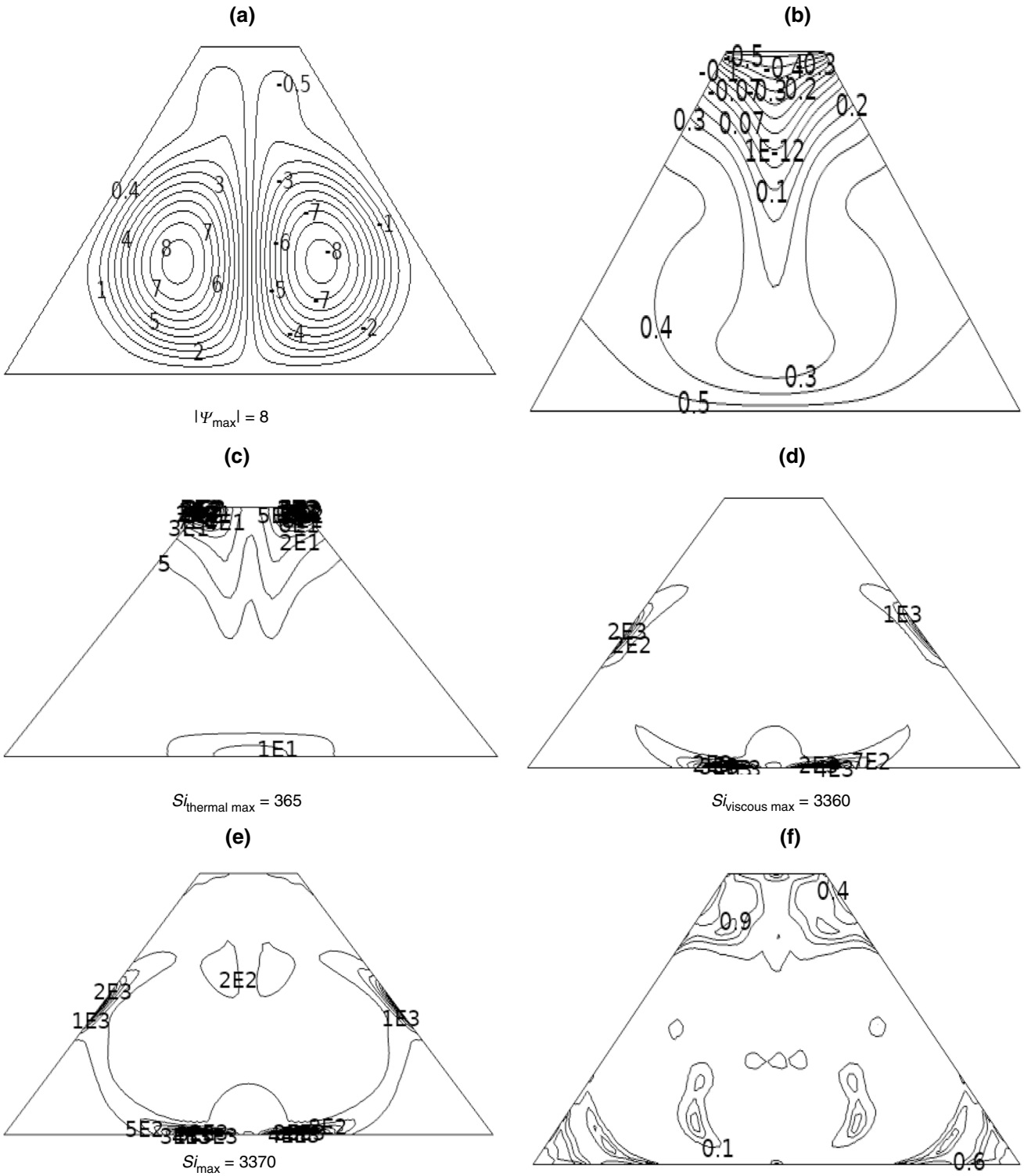

Fig. 5 Variations in **a** streamlines, **b** isotherms, **c** $Si_{Thermal}$, **d** $Si_{Viscous}$, **e** Si and **f** Be contours at AR = 0.50, Ra = 10^5, and $\phi = 10^{-4}$

aspect ratio of cavity convection dominates over conduction due to availability of space occurs in domain. The irreversibility phenomenon related to fluid friction and local entropy decreases with increasing AR, while a slight rise in the irreversibility of heat transport is seen when $(Si_{Themal})_{Max}$, $(Si_{Viscous})_{Max}$, and $(Si)_{Max}$ which is shown in Fig. 6c–f. From these sketches, it is found that as the aspect ratio increases,

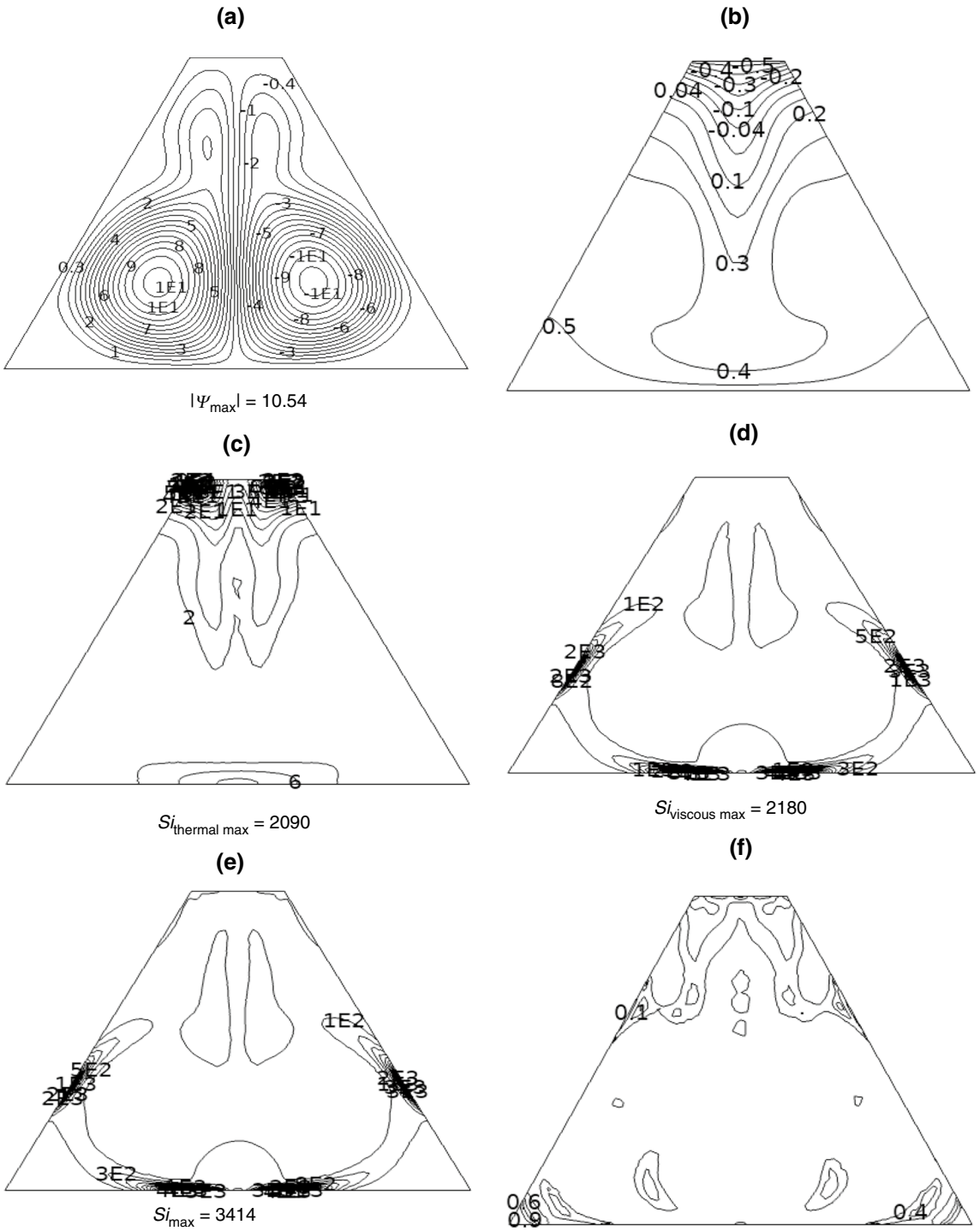

Fig. 6 Variations in **a** streamlines, **b** isotherms, **c** $Si_{Thermal}$, **d** $Si_{Viscous}$, **e** Si and **f** Be contours at AR = 0.75, Ra = 10^5, and $\phi = 10^{-4}$

the flow becomes more stable which reduces the turbulence and energy dissipation associated with fluid friction. As an outcome entropy generation due to fluid friction and local entropy decreases whereas, thickness of thermal boundary layer near the hot wall increases which lead to decrease in the convective heat transfer coefficient and thus the entropy due to heat transfer rises.

Variation in total thermal entropy ($Si_{Total\ Thermal}$), total viscous entropy ($Si_{Total\ Viscous}$), total entropy (Si_{Total}) and average Bejan number (Be_{Avg}) against aspect ratio (AR) varies from 0.25 to 0.75 for different magnitudes of Rayleigh number

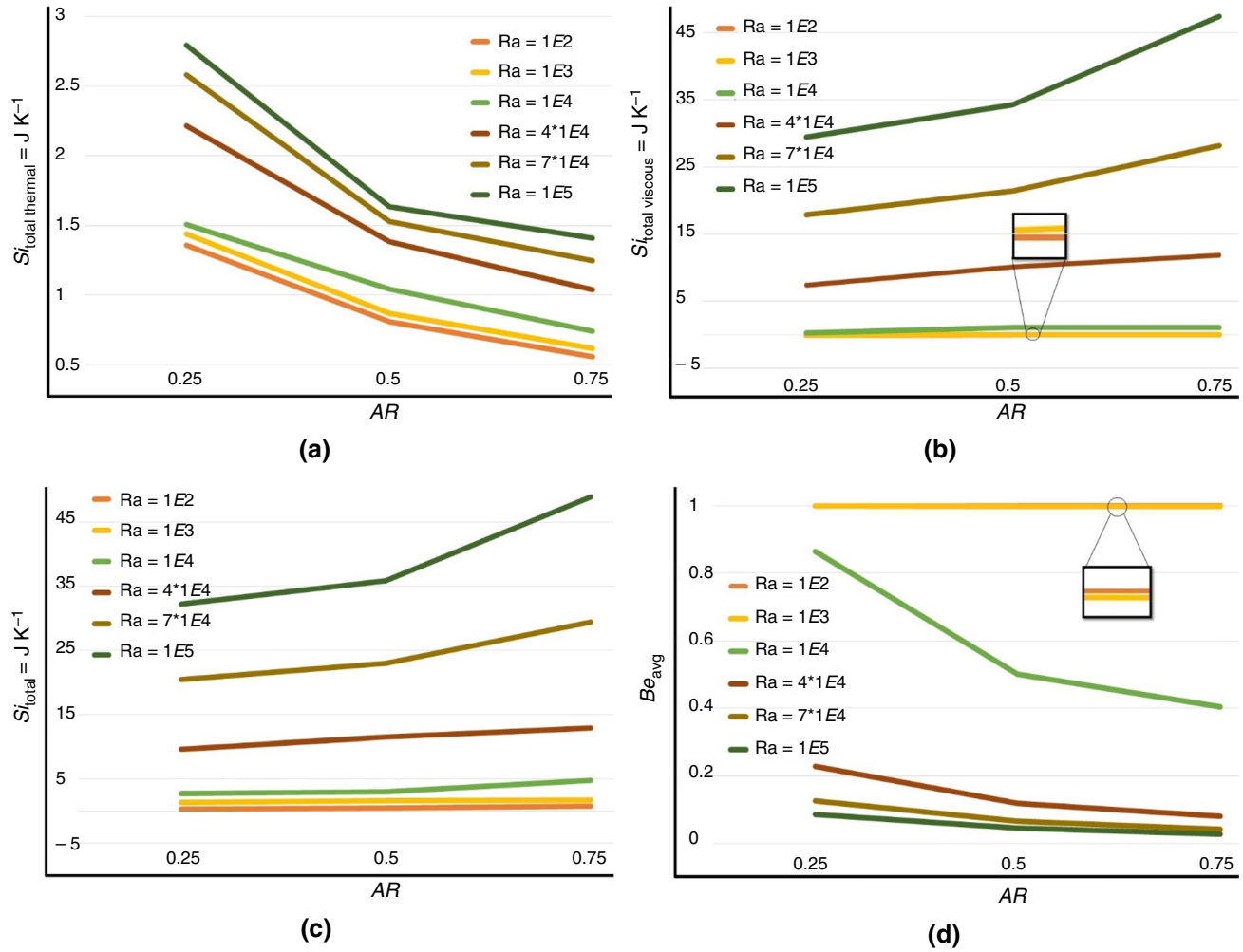

Fig. 7 Variations in **a** $Si_{TotalThermal}$, **b** $Si_{TotalViscous}$, **c** Si_{Total}, and **d** Be_{Avg} against aspect ratio (AR) for various values of Ra at $\phi = 10^{-4}$

($10^2 \leq Ra \leq 10^5$) is demonstrated in Fig. 7a–d by keeping the magnitude of irreversibility ratio and Prandtl number fixed at ϕ=10^{-4} and Pr = 0.71, respectively. In Fig. 7a variation in ($Si_{Total\ Thermal}$) against change in aspect ratio (AR) and Rayleigh number (Ra) is demonstrated. To interpret their impact in exclusive manner (AR) is varied from 0.25 to 0.75 and (Ra) is changed from 10^2 to 10^5. Decrease in ($Si_{Total\ Thermal}$) is found against (AR), whereas increasing aspects in it are observed against (Ra). Quantitively, 47% decrement is delineated in ($Si_{Total\ Thermal}$) and magnitude of total thermal entropy reduces from 2.7969 to 1.4580 against (AR) change from 0.25 to 0.75. The reason behind decaying aspect total thermal entropy versus positive change in (AR) is justified by the argument that when (AR) increases the distance between hot (bottom) and cold (top) walls elevates due to which temperature gradient diminishes and leads to cause reduction in ($Si_{Total\ Thermal}$). Figure 7b expresses deviation in ($Si_{Total\ Viscous}$) against aspect ratio for different Rayleigh number is displayed. Rise in total viscous entropy is observed for different magnitudes of (AR) and for all values of (Ra). Physically, it is justified that enlargement in (AR) from 0.25 to 0.75 leads to the development high shear forces along the wall and contributes to viscous dissipation, as a consequence ($Si_{Total\ Viscous}$) upsurges. Increasing effect of (Ra) on total viscous entropy is due to the production of fluid flow caused by generation of temperature gradient at Ra = 10^5. The influence in total entropy (Si_{Total}) is illustrated in Fig. 7c. It is revealed that, as the amplitude of (AR) rises from 0.25 to 0.75, the geometry of the enclosure enlarges which causes large and more complex flow patterns as a result the magnitude of (Si_{Total}) upsurges and the highest value of 48.885 is obtained. Subsequently, Fig. 7d deliberates variations in average Bejan number (Be_{Avg}) against (AR) for various magnitudes of (Ra). As the average Bejan number is a dimensionless quantity which determine the relative importance of entropy due heat transfer and fluid friction in a system. A higher Bejan number, i.e., (Be > ½) indicates that

entropy due to heat transfer is dominants over entropy due to fluid friction, whereas for (Be < ½) fluid friction is more dominant. It is manifested from Fig. 7d that as the magnitude of (AR) increases, the cavity becomes larger in the vertical direction (H) relative to the horizontal direction (L) which leads to a decrease in the strength of the buoyancy-driven convective flows, which is the primary mechanism for heat transfer in natural convection. As the natural convection flow weakens, the heat transfer rate within the cavity decreases, which lead to a lower ($Si_{Total\ Thermal}$) and consequently, the magnitude (Be_{Avg}) would decreases. Moreover, opposite trend in average Bejan number is depicted against (Ra) in comparison the variation in (AR). As the amplitude of (Ra) upsurges from 10^2 to 10^5, the magnitude of (Be_{Avg}) down surges. Moreover, at lower magnitudes of Ra (10^2 and 10^3) the strength of (Be_{Avg}) is greater than ½ which indicates that the irreversibility is due to heat transfer whereas, for high magnitudes of Ra (4×10^4, 7×10^4, and 10^5), the value of (Be_{Avg}) is less than ½ which shows that the irreversibility due to fluid friction is strengthen then thermal entropy.

Variation of total thermal entropy ($Si_{Total\ Thermal}$), total viscous entropy ($Si_{Total\ Viscous}$), total entropy (Si_{Total}), and average Bejan number ($Be_{Average}$) against aspect ratio (AR) varies from 0.25 to 0.75 for various values of Rayleigh number, i.e., ($Ra = 10^2$ to 10^5) is demonstrated in Fig. 8a–d, by keeping fixed irreversibility ratio ($\phi = 10^{-2}$) and Prandtl number (Pr = 0.71). In Fig. 8a, variations of ($Si_{Total\ Thermal}$) is shown against aspect ratio for different values of Rayleigh number. It is noticed that, as the value of (AR) increases, the magnitude of ($Si_{Total\ Thermal}$) decreases. Numerically, the highest magnitude 2.8 of total thermal entropy is achieved at (AR = 0.25). This declined in the magnitude of ($Si_{Total\ Thermal}$) is caused by the larger gap generated between heated (bottom) and cold (top) walls of the enclosure which lead to weaker temperature gradient outcomes flow intensity and heat transfer reduced. In addition, variations in total

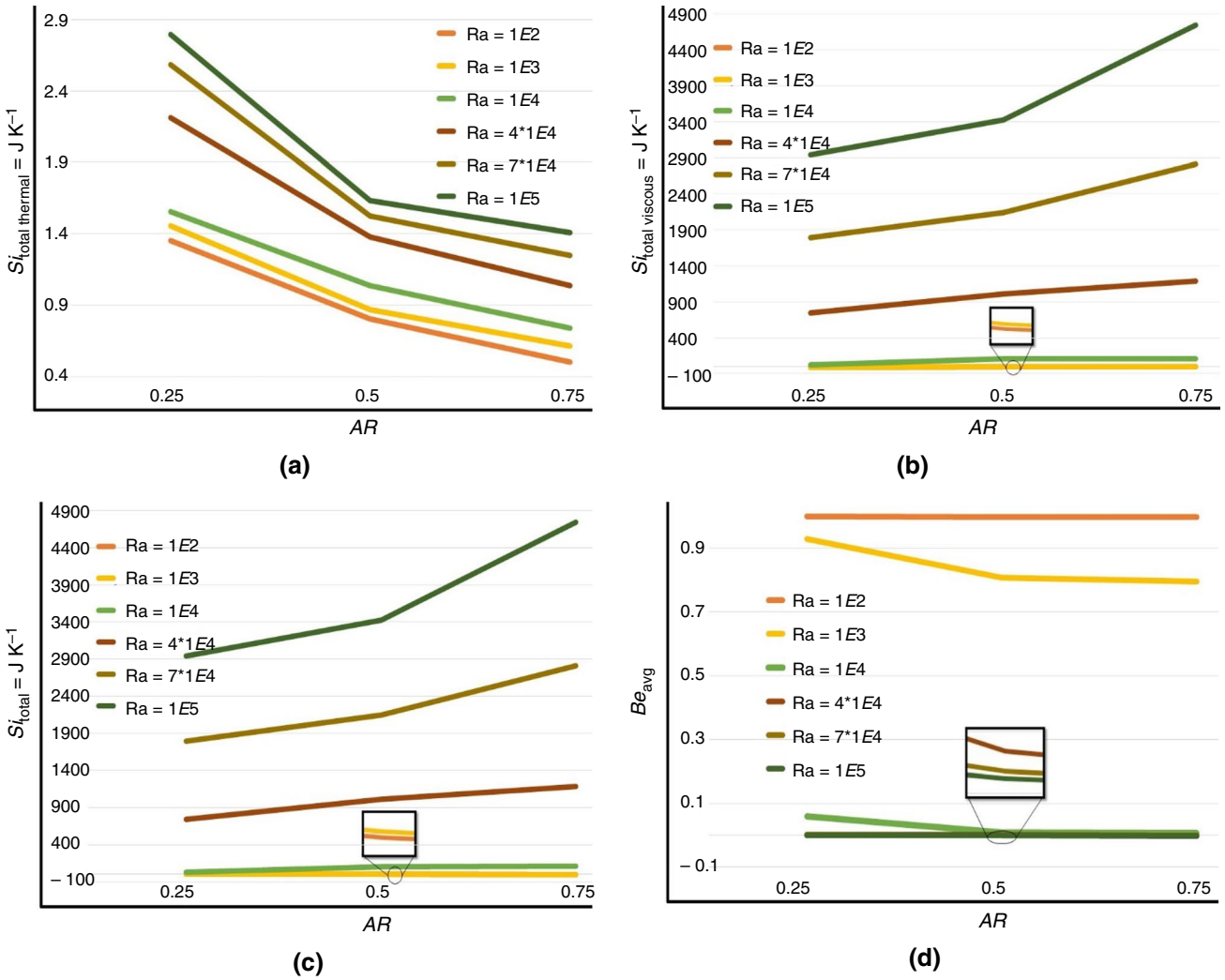

Fig. 8 Variations in **a** $Si_{TotalThermal}$, **b** $Si_{TotalViscous}$, **c** Si_{Total}, and **d** Be_{Avg} against aspect ratio (AR) for different values of Ra at $\phi = 10^{-2}$.

viscous entropy against aspect ratio for different Rayleigh number is depicted in Fig. 8b. It is revealed that, the magnitude of ($Si_{Total\ Viscous}$) upsurges as the amplitude of (AR) and (Ra) rises. This increment in the magnitude of total viscous entropy against aspect ratio is caused by larger space generated between thermal walls which allows fluid to circulate and fluid motion increases, which leads to produce higher shear rates and fluid velocities, as an outcomes viscous dissipation upsurge. Furthermore, a repaid incrementing behavior of total viscous entropy at high magnitude of ($Ra = 10^5$) is due to the growth of the fluid flow whereas, less incrementing performance is noted at low values of ($Ra = 10^2$) due to dominancy of viscous forces over inertial and minimal effects of buoyancy-induced turbulence. Moreover, variations in (Si_{Total}) against (AR) for different values of (Ra) is illustrated in Fig. 8c. It is noticed that, as the amplitude of Rayleigh number rises, the magnitude of total entropy also increases. Quantitatively, the maximum magnitude of (Si_{Total}) is 4748.9 obtained at ($Ra = 10^5$). This augmentation, is produced by dominancy of total viscous entropy over total thermal entropy and (Si_{Total}) looks like ($Si_{Total\ Viscous}$). Subsequently, deviations in average Bejan number (Be_{Avg}) against aspect ratio and Rayleigh number is delineated in Fig. 8d. It is depicted that, the values of (Be_{Avg}) declined against the upsurges magnitude of (AR). This decrement in the values of average Bejan number is caused by weaker buoyant forces which leads to lower fluid motion and potentially reduces heat transfer. Moreover, at lower magnitude of ($Ra = 10^2$) the strength of (Be_{Avg}) is greater than ½ which indicates that the irreversibility is due to heat transfer, whereas for higher magnitude of ($Ra = 10^5$) the amplitude of (Be_{Avg}) less than ½ which shows the irreversibility due to fluid friction is overriding on irreversibility due to heat transfer.

Variations local Nusselt number (Nu_{Local}) against Rayleigh number (Ra) for various values of aspect ratio (AR) of cavity is deliberated in Fig. 9. It is revealed that (Nu_{Local})

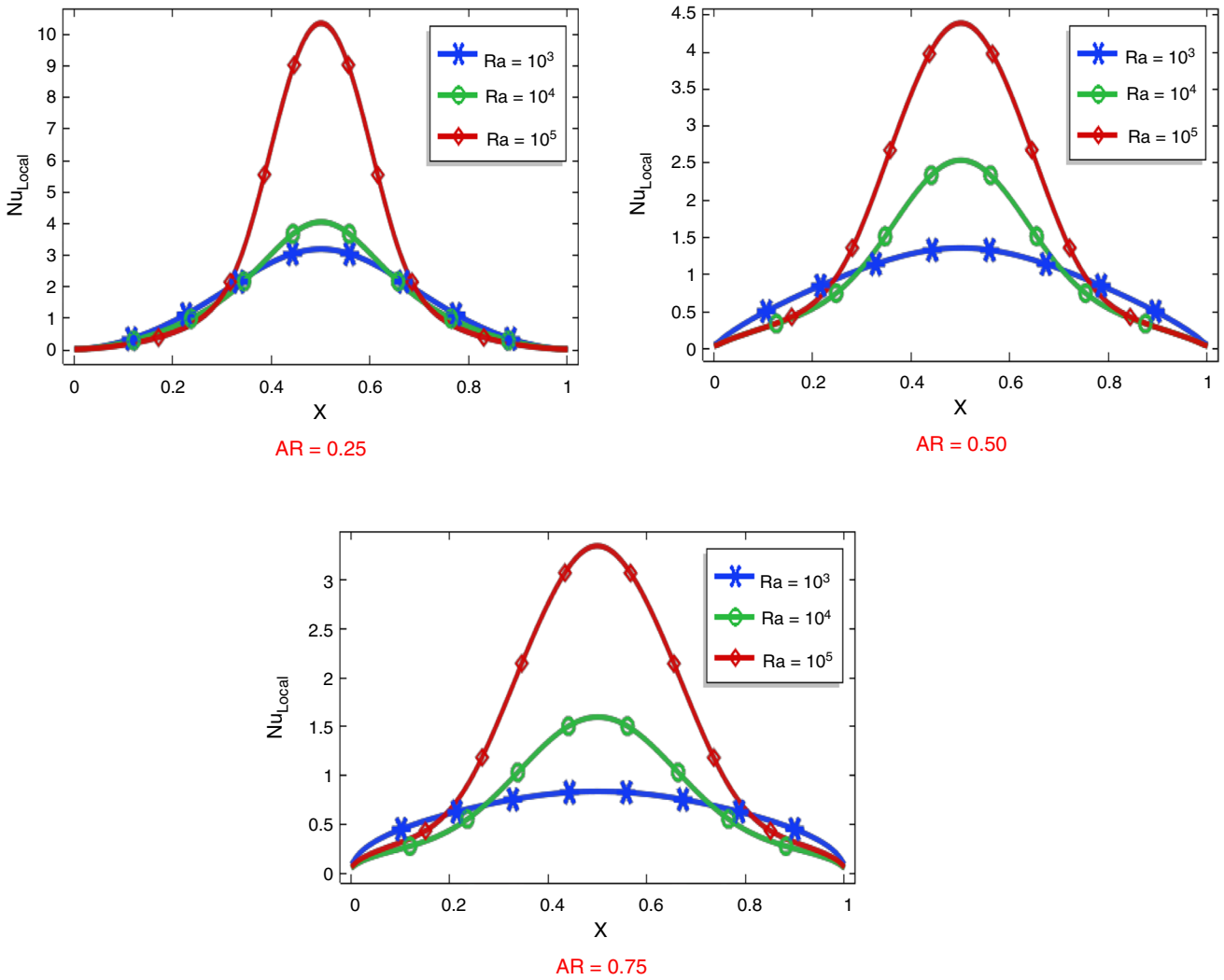

Fig. 9 Variations in local Nusselt number (Nu_{Local}) against Ra for difference AR

Table 3 Variation in average Nusselt number and ECOP against Ra for three different aspect ratios AR

Ra	AR = 0.25		AR = 0.50		AR = 0.75	
	Nu_{Avg}	ECOP	Nu_{Avg}	ECOP	Nu_{Avg}	ECOP
10^3	1.4582	0.999246	0.8693	0.998277	0.6182	0.997515
10^4	1.5060	0.864722	1.0414	0.501904	0.7404	0.40422
10^5	2.7999	0.086937	1.6400	0.045726	1.4188	0.029025

show increasing behavior against Ra. As the Ra rises, the buoyancy forces become dominant over the viscous which causes buoyancy-driven convection becomes stronger. As a result, fluid motion and heat transfer near the surface increased. Consequently, the convective heat transfer is measured by the (Nu_{Local}) also increase. Furthermore, it is also manifested that, the (Nu_{Local}) declines against the value of AR of the cavity. As the value of AR rises more space is generated for fluid motion in the cavity which reduce the heat transfer and fluid mixing. This weaken heat transport and mixing lower the convective heat transfer coefficient, which decrease the (Nu_{Local}).

Variation in average Nusselt number ($Nu_{Average}$) and ecological coefficient of performance (ECOP) against Rayleigh number (Ra) for different aspect ratios (AR) of enclosure is enumerated in Table 3. During the calculation of mention physical quantities Prandtl number (Pr) and irreversibility ratio (ϕ) are unchanged at 0.71 and 10^{-4}, respectively. In addition, wide range of flow controlling parameters are entertained such as $10^3 \leq Ra \leq 10^5$ and $0.25 \leq AR \leq 0.75$. It is noticed that by increasing (Ra) from 10^3 to 10^5, ($Nu_{Average}$) escalates, whereas opposite trend is exhibits against rising value of AR from 0.25 to 0.75. Extensive growth in the magnitude of ($Nu_{Average}$) up to 47.91%, 46.99%, and 56.42% is experienced when (Ra) increased from 10^3 to 10^5 at AR = 0.25, 0.50, and 0.75, respectively. Moreover, as AR increases from 0.25 to 0.75, the space between the heated and cold walls increases, this gap reduces the area through which heat can be exchanged between the fluid and the walls, leading to decrease in convective heat transfer efficiency and as an outcome 57.60%, 50.83%, and 49.32% declined is observed in magnitude of ($Nu_{Average}$) at $Ra = 10^3$, 10^4, and 10^5. Additionally, ecological coefficient of performance (ECOP) which indicates the thermal performance of a computational domain is thus measured against flow controlling parameters. Higher magnitude of (ECOP) represents that minimization in the entropy of the system, whereas lower value of (ECOP) exhibits reduced heat transfer rate due thermal convection. The magnitude of (ECOP) down surges against rising amplitudes of both Ra and AR. Optimum value of (ECOP), i.e., 0.999246 is perceived when Ra is minimum i.e. (10^3) as compared to the scenario when Ra is maximum, i.e., (10^5) at AR = 0.25.

Concluding remarks

Examination about influence of change in aspect ratio of trapezoidal enclosure on entropy generation in the flow of viscous fluid is analyzed. Two different types of entropy including, thermal and viscous are measured against involved physical parameters. Subsequently, Bejan number determining the ratio of thermal to local entropies is also estimated which delineates the dominance of convection and conduction transport regimes. Finite element approach via COMSOL Multiphysics software is utilized to execute numerical simulations.

Some exclusive outcomes of current communication are addressed as below

1. Depreciation in thermal entropy appears against increase in aspect ratio of enclosure, whereas all other associated entropies depict elevation.
2. At $Ra = 10^5$, the magnitude of Bejan number approaches toward unity which signifies the dominance of convection over conduction in contrary to the situation at low thermal Rayleigh number.
3. For $Ra < 10^4$ no appreciable change in viscous and thermal entropies is found, whereas at $Ra > 10^4$, comprehensive growth in mentioned quantities is measured.
4. Magnitude of viscous entropy is more in case of high value of irreversibility ratio, i.e., $\phi = 10^{-2}$ in comparison to lower magnitude of (ϕ).
5. By increasing (Ra), total entropy formulation rises in the enclosure and for a similar *Ra*, an enclosure with a high aspect ratio (i.e., AR = 0.75) may generate less total entropy than a cavity with a low aspect ratio (i.e., AR = 0.25).
6. For high Rayleigh number (i.e., $Ra = 10^5$), the magnitude of (Be_{Avg}) is less than ½, which indicates the dominance of entropy generation due to fluid friction, whereas for low Rayleigh number ($Ra = 10^2$), the magnitude of (Be_{Avg}) is greater than ½, which shows the effectiveness of heat transfer in generating irreversibility phenomena.
7. 64.76% and 49.32% decrease are obtained in local Nusselt number and average Nusselt number, respectively, when aspect ratio (AR) is increased from 0.25 to 0.75 at ($Ra = 10^5$).

8. It is noticed that ECOP reduces against increment in (AR), which also evidences minimization in entropy arises due to aspect ratio change.

Funding Open access funding provided by the Scientific and Technological Research Council of Türkiye (TÜBİTAK).

References

1. Dagtekin I, Oztop HF, Bahloul A. Entropy generation for natural convection in Γ-shaped enclosures. Int Commun Heat Mass Transfer. 2007;34(4):502–10.
2. Magherbi M, Abbassi H, Brahim AB. Entropy generation at the onset of natural convection. Int J Heat Mass Transf. 2003;46(18):3441–50.
3. Yilbas BS, Shuja SZ, Gbadebo SA, Al-Hamayel HA, Boran KU. Natural convection and entropy generation in a square cavity. Int J Energy Res. 1998;22(14):1275–90.
4. Erbay LB, Altaç Z, Sülüş B. An analysis of the entropy generation in a square enclosure. Entropy. 2003;5(5):496–505.
5. Erbay LB, Altaç Z, Sülüş B. Entropy generation in a square enclosure with partial heating from a vertical lateral wall. Heat Mass Transf. 2004;40(12):909–18.
6. Cihat Baytaş A. Optimization in an inclined enclosure for minimum entropy generation in natural convection. J Non-Equilib Thermodyn. 1997. https://doi.org/10.1515/jnet.1997.22.2.145.
7. Andreozzi A, Auletta A, Manca O. Entropy generation in natural convection in a symmetrically and uniformly heated vertical channel. Int J Heat Mass Transf. 2006;49(17–18):3221–8.
8. Mahmud S, Islam AS. Laminar free convection and entropy generation inside an inclined wavy enclosure. Int J Therm Sci. 2003;42(11):1003–12.
9. Shuja SZ, Yilbas BS, Budair MO. Natural convection in a square cavity with a heat generating body: entropy consideration. Heat Mass Transf. 2000;36(4):343–50.
10. Yilbas BS. Laser short-pulse heating of gold–silver assembly: entropy generation due to heat and electricity flows in electron subsystem. Numer Heat Transf Part A Appl. 2006;49(9):873–91.
11. Ko TH. Numerical investigation of laminar forced convection and entropy generation in a helical coil with constant wall heat flux. Numer Heat Transf Part A Appl. 2006;49(3):257–78.
12. Abu-Hijleh B. Natural convection and entropy generation from a cylinder with high conductivity fins. Numer Heat Transf Part A Appl. 2001;39(4):405–32.
13. Naterer GF, Camberos JA. Entropy and the second law fluid flow and heat transfer simulation. J Thermophys Heat Transfer. 2003;17(3):360–71.
14. Cheong HT, Siri Z, Sivasankaran S. Effect of aspect ratio on natural convection in an inclined rectangular enclosure with sinusoidal boundary condition. Int Commun Heat Mass Transfer. 2013;45:75–85.
15. Ramakrishna D, Basak T, Roy S, Pop I. Analysis of heatlines during natural convection within porous square enclosures: effects of thermal aspect ratio and thermal boundary conditions. Int J Heat Mass Transf. 2013;59:206–18.
16. Sheikholeslami M, Gorji-Bandpy M, Ganji DD, Soleimani S. Natural convection heat transfer in a cavity with sinusoidal wall filled with CuO–water nanofluid in presence of magnetic field. J Taiwan Inst Chem Eng. 2014;45(1):40–9.
17. Mejri I, Mahmoudi A, Abbassi MA, Omri A. Magnetic field effect on entropy generation in a nanofluid-filled enclosure with sinusoidal heating on both side walls. Powder Technol. 2014;266:340–53.
18. Catton I. Natural convection in enclosures. In International Heat Transfer Conference Digital Library. Begel House Inc.1978.
19. de Vahl DG. Natural convection of air in a square cavity: a bench mark numerical solution. Int J Numer Meth Fluids. 1983;3(3):249–64.
20. Ostrach S. Natural convection in enclosures. J Heat Transf. 1988;110(4b):1175–90. https://doi.org/10.1115/1.3250619.
21. Emery AF, Lee JW. The effects of property variations on natural convection in a square enclosure. J Heat Transf. 1999;121(1):57–62. https://doi.org/10.1115/1.2825966.
22. Aydin O, Yang WJ. Natural convection in enclosures with localized heating from below and symmetrical cooling from sides. Int J Numer Meth Heat Fluid Flow. 2000;10(5):518–29.
23. Turan O, Poole RJ, Chakraborty N. Aspect ratio effects in laminar natural convection of Bingham fluids in rectangular enclosures with differentially heated side walls. J Nonnewton Fluid Mech. 2011;166(3–4):208–30.
24. Ganguli AA, Pandit AB, Joshi JB. CFD simulation of heat transfer in a two-dimensional vertical enclosure. Chem Eng Res Des. 2009;87:711–27. https://doi.org/10.1016/j.cherd.2008.11.005.
25. Nazarahari M, Ghasemi Asl R, Armaghani T. Experimental study of nanofluids natural convection heat transfer in various shape pores of porous media. J Therm Anal Calorim. 2024;8:1–9.
26. Subhani S, Kumar RS. Natural convection heat transfer enhancement of circular obstacle within square enclosure. J Therm Anal Calorim. 2022;147(7):4711–29.
27. Labihi A, Chehouani H, Benhamou B, Byrne P, Meslem A. New correlation for transient laminar natural convection heat transfer in a differentially heated square cavity between air and a PCM layer. J Therm Anal Calorim. 2024;18:1–5.
28. Palani N, Subhani S, Kumar RS, Dhanushkodi G. Design of finned spherical enclosures and thermal performance evaluation under natural convection. J Therm Anal Calorim. 2022;147(5):3879–88.
29. Ghosh AP, Mullick SH, Tupakula RK, Banerjee S, Singh Y, Das-Gupta D, Kundu PK. Relative analysis between step and sinusoidal temperature distribution during natural convection inside a square porous enclosure actuated from below. J Therm Anal Calorim. 2024;26:1–22.
30. Saeid NH, Pop I. Maximum density effects on natural convection from a discrete heater in a cavity filled with a porous medium. Acta Mech. 2004;171(3):203–12.
31. Poulikakos D. Maximum density effects on natural convection in a porous layer differentially heated in the horizontal direction. Int J Heat Mass Transf. 1984;27(11):2067–75.